Enhancement of Quantum Heat Engine by Encircling a Liouvillian Exceptional Point

J.-T. Bu, J.-Q. Zhang, G.-Y. Ding, J.-C. Li, J.-W. Zhang, B. Wang, W.-Q. Ding, W.-F. Yuan, L. Chen, Ş. K. Özdemir, F. Zhou, H. Jing, and M. Feng

Phys. Rev. Lett. **130**, 110402 — Published 17 March 2023

DOI: 10.1103/PhysRevLett.130.110402

Enhancement of quantum heat engine by encircling a Liouvillian exceptional point

J.-T. Bu,[1,2,*] J.-Q. Zhang,[1,*] G.-Y. Ding,[1,2,*] J.-C. Li,[1,2] J.-W. Zhang,[3] B. Wang,[1,2] W.-Q. Ding,[1,2] W.-F. Yuan,[1,2] L. Chen,[1,3] Ş. K. Özdemir,[4,†] F. Zhou,[1,3,‡] H. Jing,[5,§] and M. Feng[1,3,6,¶]

[1]*State Key Laboratory of Magnetic Resonance and Atomic and Molecular Physics, Wuhan Institute of Physics and Mathematics, Innovation Academy of Precision Measurement Science and Technology, Chinese Academy of Sciences, Wuhan 430071, China*
[2]*University of the Chinese Academy of Sciences, Beijing 100049, China*
[3]*Research Center for Quantum Precision Measurement, Guangzhou Institute of Industry Technology, Guangzhou, 511458, China*
[4]*Department of Engineering Science and Mechanics, and Materials Research Institute, Pennsylvania State University, University Park, State College, Pennsylvania 16802, USA*
[5]*Key Laboratory of Low-Dimensional Quantum Structures and Quantum Control of Ministry of Education, Department of Physics and Synergetic Innovation Center for Quantum Effects and Applications, Hunan Normal University, Changsha 410081, China*
[6]*Department of Physics, Zhejiang Normal University, Jinhua 321004, China*

Quantum heat engines are expected to outperform the classical counterparts due to quantum coherences involved. Here we experimentally execute a single-ion quantum heat engine and demonstrate, for the first time, the dynamics and the enhanced performance of the heat engine originating from the Liouvillian exceptional points (LEPs). In addition to the topological effects related to LEPs, we focus on thermodynamic effects, which can be understood by the Landau-Zener-Stückelberg process under decoherence. We witness a positive net work from the quantum heat engine if the heat engine cycle dynamically encircles an LEP. Further investigation reveals that, a larger net work is done when the system is operated closer to the LEP. We attribute the enhanced performance of the quantum heat engine to the LZS process, enabled by the eigenenergy landscape in the vicinity of the LEP, and the EP-induced topological transition. Therefore, our results open new possibilities towards LEP-enabled control of quantum heat engines and of thermodynamic processes in open quantum systems.

Quantum heat engines (QHEs), working with quantum substances, are expected to surpass the output power and efficiency of the equivalent classical counterparts by taking advantage of quantum features [1–6], such as, quantum coherence, squeezing and/or quantum correlations. The growing interest in QHEs is also fueled by the need to understand non-equilibrium thermodynamics at the nanoscale as well as the quantum-classical transition in energy-information and work-heat conversion. Efforts have been made on exploring unique characteristics of QHEs in different quantum systems [6–21].

As open quantum systems coupled to external thermal baths, QHEs can be considered as non-Hermitian quantum systems and may exhibit exceptional point (EP) degeneracies characterized by the coalescence of two or more eigenvalues and the associated eigenvectors of their non-Hermitian Hamiltonians [22–24] or Liouvillian superoperators [25]. Presence of EPs in classical and quantum systems has shown to lead to many interesting and counterintuitive phenomena such as asymmetric backscattering [26, 27], enhanced response to perturbations [28–32], and loss-induced lasing [33]. EP-related topological features have demonstrated such as state exchange [34], topological energy transfer [35], asymmetric mode switching [36–40], and phase accumulation in light-matter interactions [41, 42]. However, these studies have considered EPs of the effective Hamiltonian or equivalently the Liouvillian formalism, which involves only coherent non-unitary evolution, ignoring quantum jumps and decoherence.

To capture the full dynamics of quantum systems and lay the groundwork towards EP-enabled quantum applications and processes, one should resort to Liouvillian superoperators and their exceptional points-referred to as Liouvillian exceptional points (LEPs)-which involve the interplay of energy loss and decoherence [43]. Recently, decoherence-enhanced phenomena near LEPs have been studied theoretically and observed in experiments as an analogue of critical damping in classical harmonic oscillators [44–48]. These features are expected to play a role in full dynamical control of quantum thermal machines and their approach towards the steady state without additional time-dependent external drives [47].

In this Letter, we experimentally execute a QHE using a single trapped ion by encircling an LEP and witness, for the first time, an enhancement in the performance of the QHE: If the LEP is encircled during the engine cycles, an increased net positive work is obtained, whereas if the engine cycle is completed without encircling the LEP, the net work can be positive or negative. In contrast to the recent interest in the topological effects of LEPs on wave and energy transport, here we focus

on thermodynamic effects originating from an LEP. The enhancement we have observed here in the performance of the QHE due to encircling an LEP can be attributed to a Landau-Zener-Stückelberg (LZS) process [49] subject to decoherence. The Landau-Zener transition [50] occurs when a system is periodically driven through its level crossing, and the phase, commonly known as Stückelberg phase [51], accumulated between the transitions may lead to constructive or destructive interference which is referred to as LZS interferometry. Since LEPs involve both dissipation and decoherence and their encircling results in crossings between two Riemann sheets, the process may be thought as LZS under decoherence. We note that LZS in non-Hermitian systems with LEPs need further investigation to elucidate the physics involved. This, however, is beyond the scope of this study. Therefore, in the following we focus on how the performance of QHE is affected when encircling an LEP.

Our experiment is carried out on a single ultracold $^{40}Ca^{+}$ ion confined in a linear Paul trap as employed previously [52–54]. Under the pseudo-potential approximation, the axial and radial frequencies of the trap potential are, respectively, $\omega_z/2\pi = 1.0$ MHz and $\omega_r/2\pi = 1.2$ MHz. For our purpose, we employ a magnetic field of 0.6 mT directed in axial orientation, which splits the ground state $4^2S_{1/2}$ and the metastable state $3^2D_{5/2}$ into two and six hyperfine energy levels, respectively. As shown in Fig. 1(a), we encode the qubit in $|4^2S_{1/2}, m_J = +1/2\rangle$ and $|3^2D_{5/2}, m_J = +5/2\rangle$, where m_J represents the magnetic quantum number, and we label these two levels as $|1\rangle$ and $|2\rangle$, respectively. To avoid thermal phonons which are detrimental to quantum effects, we perform Doppler and sideband cooling of the ion until an average phonon number of the z-axis motional mode is much smaller than 1 with the Lamb-Dicke parameter ∼0.11. The qubit is manipulated by a narrow-linewidth Ti:sapphire laser with wavelength around 729 nm, which irradiates the ultracold ion under the carrier-transition Hamiltonian $H = \Delta|2\rangle\langle 2| + \Omega(|2\rangle\langle 1|e^{i\phi_L} + |1\rangle\langle 2|e^{-i\phi_L})/2$, with the detuning Δ and the Rabi frequency Ω taken in units of $\hbar = 1$, as shown in Fig. 1(a) and ϕ_L denoting the laser phase. In our experiment as presented below, we set Δ to vary with time and keep Ω and $\phi_L = 0$ unchanged.

To implement encircling of the LEP in the qubit (i.e, the two-level system), here we fully engineer both the drive and the dissipation with the help of the excited level $|4^2P_{3/2}, m_J = +3/2\rangle$ labeled as $|3\rangle$, which then enables us to perform the closed cycle $|1\rangle \to |2\rangle \to |3\rangle \to |1\rangle$, see Fig. 1(a). The first step $|1\rangle \to |2\rangle$ is achieved using the Ti:sapphire laser (729-nm) tuned exactly to the resonance transition. The second step from $|2\rangle$ to $|3\rangle$ is a dipolar transition mediated using a semiconductor laser (854-nm) under the restriction of the selection rule. The third step $|3\rangle \to |1\rangle$ takes place as spontaneous emission which is also restricted by the selection rule. Practically, by tuning the 729-nm and 854-nm lasers under the condition of $\Omega \ll \tilde{\Omega}$, we may transform this three-level configuration into an effective two-level system spanned by $|1\rangle$ and $|2\rangle$ whose Rabi frequency Ω and the effective decay rate $\gamma_{\rm eff} = \tilde{\Omega}^2/\Gamma$ is fully tunable [55].

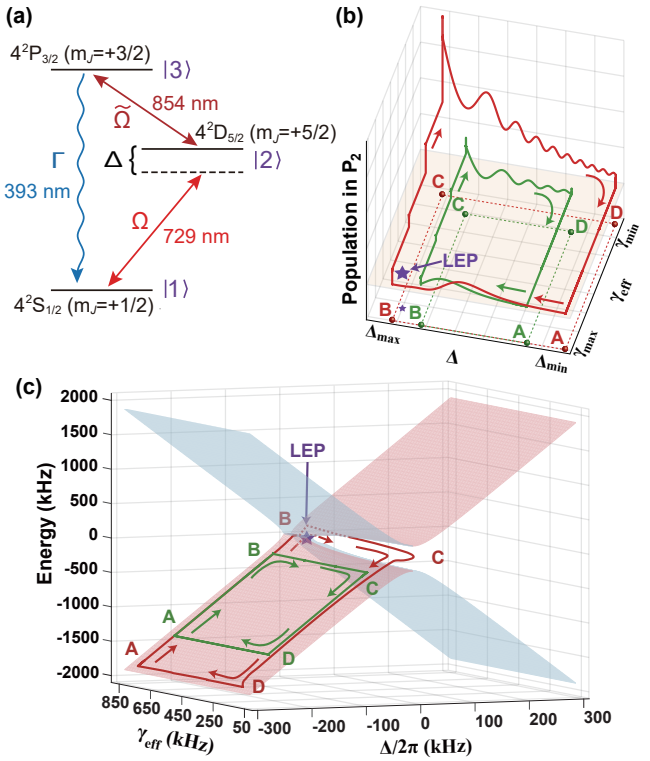

FIG. 1: (a) Level scheme of $^{40}Ca^{+}$ ion, where the solid arrows represent the transitions driven by lasers with Rabi frequencies Ω ($\tilde{\Omega}$) for the 729-nm (854-nm) laser and detuning Δ for the 729-nm laser. The wavy arrow represents spontaneous emission with decay rate Γ. (b) Simulations of the populations in $|2\rangle$ with respect to the detuning Δ and the effective decay rate $\gamma_{\rm eff}$, where the red (green) solid curve represents the evolution of the population with (without) the LEP encircled. The dashed curves are the projection of the solid curves with the same color on the bottom plane for guiding eyes. The four corner points A, B, C, and D are labeled for convenience of description in the text. The LEP is labeled by the purple star. (c) Illustration of trajectories with and without encircling the LEP on the Riemann surface, corresponding to the QHE cycles plotted by the solid lines with the same color in (b). In contrast to the green curve, representing the trajectory without encircling the LEP and localized just in one branch of the Riemann surface, the red curve encircling the LEP passes through the two branches (the dashed part denotes the track in the other branch), leading to the topological properties that are relevant to the thermodynamic effects observed in the present experiment.

The dynamics of this effective two-level model is described by the Lindblad master equation,

$$\dot{\rho} = \mathcal{L}\rho, \tag{1}$$

where $\mathcal{L}$ is the Liouvillian superoperator, ρ denotes the density operator, and $\mathcal{L}\rho \equiv -i[H,\rho]+\frac{\gamma_{\rm eff}}{2}(2|1\rangle\langle 2|\rho|2\rangle\langle 1|-|2\rangle\langle 1||1\rangle\langle 2|\rho-\rho|2\rangle\langle 1||1\rangle\langle 2|)$. The physics of the LEPs can be understood from the eigensolutions of $\mathcal{L}$ at $\Delta = 0$, given by $\lambda_1 = 0$, $\lambda_2 = -\gamma_{\rm eff}$, $\lambda_3 = (-3\gamma_{\rm eff} - \xi)/4$, and $\lambda_4 = (-3\gamma_{\rm eff} + \xi)/4$, with $\xi = \sqrt{\gamma_{\rm eff}^2 - 16\Omega^2}$ [56]. When $\xi = 0$, that is $\gamma_{\rm eff} = 4\Omega$, the eigenvalues λ_3 and λ_4 merge, giving rise to a second order LEP at $\tilde{\lambda} = -3\gamma_{\rm eff}/4$. Clearly, for $\gamma_{\rm eff} > 4\Omega$ (weak coupling), both λ_3 and λ_4 are real with a splitting amount ξ, corresponding to the broken phase characterized by a non-oscillatory dynamics with purely exponential decay [60, 61]. For $\gamma_{\rm eff} < 4\Omega$ (strong coupling), on the other hand, λ_3 and λ_4 form a complex conjugate pair which splits in their imaginary parts by ξ, corresponding to the exact phase characterized by an oscillatory dynamics. Thus, the LEP represents a topological transition point between the exact and the broken phases, dividing the parameter space into a region of oscillatory dynamics ($\gamma_{\rm eff} < 4\Omega$) and a region of non-oscillatory dynamics ($\gamma_{\rm eff} > 4\Omega$).

In our experiment, we execute a QHE cycle consisting of four strokes, as plotted in Fig. 1(b). The first stroke which is implemented by increasing the detuning Δ linearly from its minimum value $\Delta_{\rm min}$ to its maximum value $\Delta_{\rm max}$ while $\gamma_{\rm eff}$ is kept at its maximum value of $\gamma_{\rm max}$, is an iso-decay compression from A $(\Delta_{\rm min}, \gamma_{\rm max})$ to B $(\Delta_{\rm max}, \gamma_{\rm max})$. The second stroke is an isochoric heating from B $(\Delta_{\rm max}, \gamma_{\rm max})$ to C $(\Delta_{\rm max}, \gamma_{\rm min})$ and is implemented by decreasing $\gamma_{\rm eff}$ from $\gamma_{\rm max}$ to $\gamma_{\rm min}$, during which the detuning remains at $\Delta_{\rm max}$. The third stroke is an iso-decay expansion from C $(\Delta_{\rm max}, \gamma_{\rm min})$ to D $(\Delta_{\rm min}, \gamma_{\rm min})$ implemented by linearly decreasing Δ from $\Delta_{\rm max}$ to $\Delta_{\rm min}$ with $\gamma_{\rm eff} = \gamma_{\rm min}$ staying unchanged. Finally, we execute an isochoric cooling from D $(\Delta_{\rm min}, \gamma_{\rm min})$ to A $(\Delta_{\rm min}, \gamma_{\rm max})$ by increasing $\gamma_{\rm eff}$ from $\gamma_{\rm min}$ to $\gamma_{\rm max}$ while keeping Δ fixed at $\Delta_{\rm min}$. After the last stroke, we wait for the system to reach its steady state and return to its initial state in order to complete a closed cycle. For this QHE cycle, the 729-nm laser irradiation together with the real environment constitutes the hot and cold baths which correspond to $\Delta_{\rm min}$ and $\Delta_{\rm max}$, respectively. Heat exchange between the qubit and the baths is controlled by the detuning Δ (i.e., controlled by the frequency of the Ti-Sapphire laser). The strength Ω remains unchanged during the QHE cycle. Thus we may concentrate on the first and third strokes (i.e., the iso-decay processes) for scrutinizing the heat-work exchange of the QHE.

The variation of $\gamma_{\rm eff}$ in the second and fourth strokes (i.e., the isochoric processes) leads to the topological transition between the exact and broken phases. An intriguing feature of non-Hermitian systems with EPs is the topological structure of the Riemann manifold describing the complex energy of the system, which leads to state-flip (i.e., state exchange) [34] or the accumulation of a geometric phase [41] when the system parameters are tuned to encircle an EP. We note that this is true for both Hamiltonian exceptional points (HEPs) [34] and LEPs [48]. Here, our ability to tune the system parameters to complete a QHE cycle (i.e., a loop in the parameter space) enables us to complete this cycle with or without encircling the LEP (Fig. 1b). The cycle with or without encirclement of the LEP corresponds to the quantum trajectory traversing the two branches or staying on one branch of the Riemann surface (Fig. 1c). As discussed later, this unique feature, along with the dissipative LZS process, leads to higher output work from the QHE.

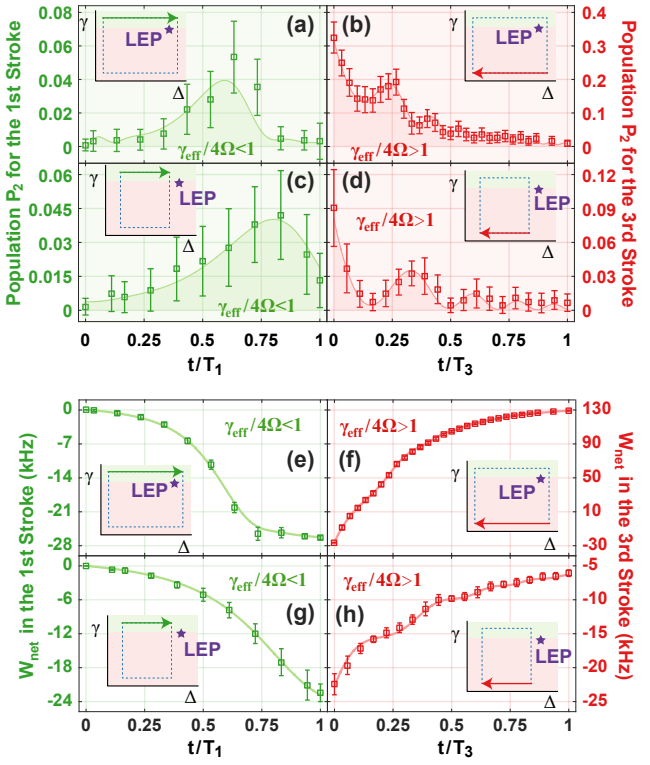

FIG. 2: Measured populations of the excited state, i.e., P_2, in iso-decay strokes, where (a) and (b) are for the first and third strokes, respectively, in the case of encircling the LEP ($\Delta_{\rm min}/2\pi = -290$ kHz, $\gamma_{\rm max} = 800$ kHz, $\Delta_{\rm max}/2\pi = 10$ kHz, $\gamma_{\rm min} = 130$ kHz). The time is set as $T_1 = T_3 = 30$ μs. (c) and (d) represent the first and third strokes, respectively, in the case of not encircling the LEP ($\Delta_{\rm min}/2\pi = -223$ kHz, $\gamma_{\rm max} = 800$ kHz, $\Delta_{\rm max}/2\pi = -43$ kHz, $\gamma_{\rm min} = 200$ kHz). The time is $T_1 = T_3 = 18$ μs. (e, f, g, h) Net work corresponding to the panels (a, b, c, d), respectively, is defined and explained in the text. In all the panels, $\Omega/2\pi$ is a constant and fixed to be 29 kHz.

Experimentally, we execute two QHE cycles as designed in Fig. 1(b) by finely tuning $\gamma_{\rm eff}$ using the Ti-sapphire and the semiconductor laser frequencies as two knobs. For convenience of description, we call the red (green) curve with (without) the LEP encircled as a big (small) cycle. To witness the thermodynamic properties, we focus on the iso-decay compression (i.e., the first

stroke) and expansion (i.e., the third stroke), in which the heat engine performs work. We first implement the big cycle. We observe a hump in the population variation in Fig. 2(a) and a population oscillation in Fig. 2(b). These suggest that the qubit is exchanging heat with the driving field [56], implying that the iso-decay strokes evolve out of adiabaticity. Since the LEP is located at $\Delta = 0$, tuning Δ back and forth through $\Delta = 0$ can be understood as an LZS process [49], where the Landau-Zener transition occurs in the first stroke with detuning varied from $\Delta_{\min}/2\pi = -290$ kHz to $\Delta_{\max}/2\pi = 10$ kHz, and the Stückelberg phase results in fringes in the reverse operation in the third stroke. However, our QHE subject to decoherence modifies the behavior of both the Landau-Zener transition and the Stückelberg interference. In contrast to the conventional Landau-Zener transition which is a non-adiabatic transition when a system traverses an avoided crossing, here during the first stroke, our systems traverses from one Riemann sheet to the other Riemann sheet (i.e., traversing avoided crossing is replaced by traversing between two Riemann sheets). The damped oscillations observed in the population variation in the third stroke of the QHE imply the presence of decoherence. Next, we implement the small cycle and observe that the hump in the population P_2 is incomplete and smaller compared to that obtained for the big cycle because in the small cycle only a non-resonance transition is involved in the process. As a result, the population variation shown in Fig. 2(d) is also weak and exhibits overdamped oscillation. It should be noted that, for convenience of comparison, we ensure the same rate of the detuning variation in both cycles. As a result, we set the implementation time $T_1 = T_3 = 30$ μs for the big cycle, while $T_1 = T_3 = 18$ μs for the small cycle.

The net work is an essential quantity for evaluating the QHE performance. We quantify the net work produced in the two QHE cycles, described above as big and small cycles, using $W_{\text{net}} = -\int_0^t \rho_c(t) dH_c$ where $\rho_c(t)$ describes the state of the two-level system governed by $H_c = \Delta(t) |2\rangle \langle 2|$. The corresponding heat in the QHE cycles is given by $Q_{\text{in(out)}} = \int_0^t H_c(t) d\rho_c$ for $d\rho_c > 0$ ($d\rho_c < 0$) [56]. Since the isochoric strokes do not perform work, here we only consider the first and third strokes. Figures 2(e) and (g) illustrate, respectively, the negative net work produced in the first strokes of the big and small cycles, indicating the fact that the baths perform work on the system in the iso-decay compression, and the Landau-Zener transition in the big cycle leads to more work acquired from the baths. Figure 2(f) and (h), on the other hand, respectively presents for the big and small cycles the amount of net work accumulated from the starting time of the third stroke counteracting the acquired work in the first stroke. Although the net work in both the big and small cycles increases, it becomes positive only for the big cycle (i.e., net work is still negative at the end of the third stroke for the small cycle). Considering the phase-induced oscillation in Fig. 2(b), we attribute the positive net work observed in Fig. 2(f) to the coherence accumulated in the Stückelberg phase.

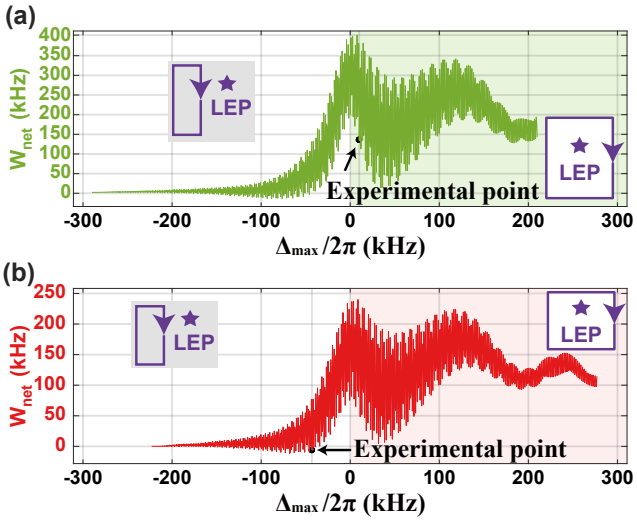

FIG. 3: Numerical simulation showing the dependence of the net work on $\Delta_{\max}$ of the QHE cycles. (a) The situation covering the big cycle of our experiment, where the QHE cycle starts from the point A with $\Delta_{\min}/2\pi = -290$ kHz and $\gamma_{\max} = 800$ kHz, sweeping the frequency to $\Delta_{\max}/2\pi \leqslant 210$ kHz. So the point C is set with -289.9 kHz $\leqslant \Delta_{\max}/2\pi \leqslant$ 210 kHz and $\gamma_{\min} = 130$ kHz. (b) The situation involving the small cycle of our experiment, where the QHE cycle starts from A with $\Delta_{\min}/2\pi = -223$ kHz and $\gamma_{\max} = 800$ kHz, sweeping the frequency to $\Delta_{\max}/2\pi \leqslant 277$ kHz. So the point C is set with -222.9 kHz $\leqslant \Delta_{\max}/2\pi \leqslant 277$ kHz and $\gamma_{\min} = 200$ kHz. In both the panels, we consider 804 points as the values of the maximal. Black dots indicate the maximal detuning of the two cycles experimentally accomplished. The points A and C referred to can be found in Fig. 1, but not labeled here for simplicity.

To justify the positive net work observed in Fig. 2 to be relevant to the LEP, we numerically evaluate the net work of the two QHE cycles in different variations of the detuning in the first and third strokes, checking if W_{net} can remain positive once the LEP is enclosed in the QHE cycle. To this end, we fix the point A, i.e., the value of $\Delta_{\min}$ to be the same as in Fig. 2, but consider different values of $\Delta_{\max}$ in the calculation of the first and third strokes. In addition, the effective decays in the second and fourth strokes are varied between 130 kHz and 800 kHz, also the same as in Fig. 2. Since the maximal values of $\Delta_{\max}$ considered here are much larger than those considered in the experiments, this numerical result helps understand what happens in our experimental observation. The numerical simulation in Fig. 3 indicates

clearly that $W_{\rm net}$ can be positive or negative if the LEP is not encircled; while it is always positive if the LEP is enclosed in the QHE cycle. Moreover, Fig. 3 shows that the net work is larger for the loop closer to the LEP.

Our analysis above neglects the second and fourth strokes which are relevant to the topological transition between the exact and the broken phases induced by the LEP. Although no work is generated during the second and fourth strokes, the topological transitions occurred during the encircling of the LEP in these two strokes, as parts of the QHE cycle, play an important role in the enhancement of the QHE performance. In Fig. 2, we see the association of the positive net work with the higher population observed in the big cycle. Since lowering γ in the second stroke of the big cycle, leading to the topological transition from the broken phase to the exact phase, helps increasing the population P_2 (see Fig. 1b in comparison with the small cycle), we attribute the enhanced performance of the QHE to LZS-enabled thermodynamic effects and the topological transition regarding the LEP. We also note that previous experimental demonstrations considered topological effects induced by encircling EPs [62–64], but not LEPs. In this paper, we have established a link between the performance of a QHE and the topological effects originating from encircling an LEP.

In conclusion, we have executed the first QHE by dynamically encircling a LEP in a single trapped-ion system. The positive net work in this QHE originates from the LZS process and the topological transition across the LEP. Thus, the LEP represents a proper description of both the topological and the thermodynamical effects involved in the QHE cycles. These results help understand thermodynamic effects in non-Hermitian quantum systems exhibiting EPs and the roles of quantum effects in heat-work conversion and working substance-bath interaction in heat engines. Our results are not limited to trapped ions and can be extended to other quantum thermodynamic systems, such as heat engines utilizing superconducting qubits (i.e., emergence of a LEP in a transmon qubit system has been reported [45, 64]). We note that one could couple quantum loads to the working substance (i.e., here a trapped ion) to convert the work produced by the heat engine into useful energy for storage and further processing [65]. This would give a deeper insight into LEP-associated thermodynamic effects in quantum systems and open new possibilities towards non-Hermitian thermodynamic control of open quantum systems for practical technologies, such as quantum probes and quantum computing.

This work was supported by Special Project for Research and Development in Key Areas of Guangdong Province under Grant No. 2020B0303300001, by National Natural Science Foundation of China under Grant Nos. U21A20434, 12074390, 12074346, 11835011, 11734018, by Key Lab of Guangzhou for Quantum Precision Measurement under Grant No.202201000010, and by Postdoctoral Science Foundation of China under Grant No. 2022MT10881. Ş.K.Ö acknowledges the support from Air Force Office of Scientific Research (AFOSR) Multidisciplinary University Research Initiative (MURI) Award No. FA9550-21-1-0202.

* Co-first authors with equal contribution
† Electronic address: sko9@psu.edu
‡ Electronic address: zhoufei@wipm.ac.cn
§ Electronic address: jinghui73@foxmail.com
¶ Electronic address: mangfeng@wipm.ac.cn

[1] J. Gemmer, M. Michel, & G. Mahler, Quantum Thermodynamics (Springer, Berlin Heidelberg New York, 2004).
[2] M. O. Scully, M. S. Zubairy, G. S. Agarwal, & H. Walther, Extracting Work from a Single Heat Bath via Vanishing Quantum Coherence, *Science* **299**, 862 (2003).
[3] J. M. R. Parrondo, J. M. Horowitz, & T. Sagawa, Thermodynamics of information, *Nat. Phys.* **11**, 131 (2015).
[4] G. Alvarado Barrios, F. Albarrán-Arriagada, F. A. Cárdenas-López, G. Romero, & J. C. Retamal, Role of quantum correlations in light-matter quantum heat engines, *Phys. Rev. A* **96**, 052119 (2017).
[5] A. Hewgill, A. Ferraro, & G. De Chiara, Quantum correlations and thermodynamic performances of two-qubit engines with local and common baths, *Phys. Rev. A* **98**, 042102 (2018).
[6] J. Klatzow, J. N. Becker, P. M. Ledingham, C. Weinzetl, K. T. Kaczmarek, D. J. Saunders, J. Nunn, I. A. Walmsley, R. Uzdin, & E. Poem, Experimental Demonstration of Quantum Effects in the Operation of Microscopic Heat Engines, *Phys. Rev. Lett.* **122**, 110601 (2019).
[7] E. Muñoz & F. J. Peña, Quantum heat engine in the relativistic limit: The case of a Dirac particle, *Phys. Rev. E* **86**, 061108 (2012).
[8] M. O. Scully, K. R. Chapin, K. E. Dorfman, M. B. Kim, & A. Svidzinsky, Quantum heat engine power can be increased by noise-induced coherence, *Proc. Natl. Acad. Sci. U.S.A.* **108**, 15097 (2011).
[9] J. Roβnagel, O. Abah, F. Schmidt-Kaler, K. Singer, & E. Lutz, Nanoscale Heat Engine Beyond the Carnot Limit, *Phys. Rev. Lett.* **112**, 030602 (2014).
[10] A. Ü. C. Hardal and Ö. E. Müstecaplioğlu, Superradiant Quantum Heat Engine, *Sci Rep.* **5**, 12953 (2015).
[11] J. Roβnagel, S. T. Dawkins, K. N. Tolazzi, O. Abah, E. Lutz, F. Schmidt-Kaler, & K. Singer, A single-atom heat engine, *Science* **352**, 325 (2016).
[12] G. Maslennikov, S. Q. Ding, R. Hablutzel, J. Gan, A. Roulet, S. Nimmrichter, J. Dai, V. Scarani, & D. Matsukevich, Quantum absorption refrigerator with trapped ions, *Nat. Commun.* **10**, 202 (2019).
[13] D. von Lindenfels, O. Gräb, C. T. Schmiegelow, V. Kaushal, J. Schulz, M. T. Mitchison, J. Goold, F. Schmidt-Kaler, & U. G. Poschinger, Spin Heat Engine

Coupled to a Harmonic-Oscillator Flywheel, *Phys. Rev. Lett.* **123**, 080602 (2019).

[14] C. A. Ryan, O. Moussa, J. Baugh, & R. Laflamme, Spin Based Heat Engine: Demonstration of Multiple Rounds of Algorithmic Cooling, *Phys. Rev. Lett.* **100**, 140501 (2008).

[15] J. P. S. Peterson, T. B. Batalhão, M. Herrera, A. M. Souza, R. S. Sarthour, I. S. Oliveira, & R. M. Serra, Experimental Characterization of a Spin Quantum Heat Engine, *Phys. Rev. Lett.* **123**, 240601 (2019).

[16] J. V. Koski, V. F. Maisi, J. P. Pekola, & D. V. Averin, Experimental realization of a Szilard engine with a single electron, *Proc. Natl. Acad. Sci. U.S.A.* **111**, 13786 (2014).

[17] K. Ono, S. N. Shevchenko, T. Mori, S. Moriyama, & F. Nori, Analog of a Quantum Heat Engine Using a Single-Spin Qubit, *Phys. Rev. Lett.* **125**, 166802 (2020).

[18] H. T. Quan, Y. D. Wang, Y. X. Liu, C. P. Sun, & F. Nori, Maxwell Demon Assisted Thermodynamic Cycle in Superconducting Quantum Circuits, *Phys. Rev. Lett.* **97**, 180402 (2006).

[19] A. Guthrie, C. D. Satrya, Y.-C. Chang, P. Menczel, F. Nori, J. P. Pekola, A Cooper-Pair Box Architecture for Cyclic Quantum Heat Engines, *PhysRevApplied* **17**, 064022 (2022).

[20] K. Zhang, F. Bariani, P. Meystre, Quantum optomechanical heat engine, *Phys. Rev. Lett.* **112**, 150602 (2014).

[21] A. Dechant, N. Kiesel, & E. Lutz, All-Optical Nanomechanical Heat Engine, *Phys. Rev. Lett.* **114**, 183602 (2015).

[22] Markus Müller, & I. Rotter, Exceptional points in open quantum systems, *J. Phys. A: Math. Theor.* **41**, 244018 (2008).

[23] M.-A. Miri & A. Alú, Exceptional points in optics and photonics, *Science* **363**, 42 (2019).

[24] Ş. K. Özdemir, S. Rotter, F. Nori, & L. Yang, Parity-time symmetry and exceptional points in photonics, *Nat. Mater.* **18**, 783 (2019).

[25] A. Insinga, B. Andresen, P. Salamon, & Ronnie Kosloff, Quantum heat engines: Limit cycles and exceptional points, *Phys. Rev. E* **97**, 062153 (2018)

[26] B. Peng, Ş. K. Özdemir, M. Liertzer, W. Chen, J. Kramer, H. Yilmaz, J. Wiersig, S. Rotter, & L. Yang Chiral modes and directional lasing at exceptional points, *Proc. Natl. Acad. Sci.* **113**, 25 (2016).

[27] S. Soleymani, Q. Zhong, M. Mokim, S. Rotter, R. El-Ganainy & Ş. K. Özdemir, Chiral and degenerate perfect absorption on exceptional surfaces, *Nat. Commun.* **13**, 599 (2022).

[28] H. Hodaei, A. U. Hassan, S. Wittek, H. Garcia-Gracia, R. El-Ganainy, D. N. Christodoulides, & M. Khajavikhan, Enhanced sensitivity at higher-order exceptional points, *Nature (London)* **548**, 187 (2017).

[29] W. Chen, Ş. K. Özdemir, G. Zhao, J. Wiersig & L. Yang, Exceptional points enhance sensing in an optical microcavity, *Nature (London)* **548**, 192 (2017).

[30] J. Wiersig, Review of exceptional point-based sensors, *Photon. Res.* **8**, 1457 (2020)

[31] Y.-H. Lai, Y.-K. Lu, M.-G Suh, Z. Yuan & K. Vahala, Observation of the exceptional-point enhanced Sagnac effect, *Nature (London)* **576**, 65 (2019).

[32] M. P. Hokmabadi, A. Schumer, D. N. Christodoulides, & M. Khajavikhan, Non-Hermitian ring laser gyroscopes with enhanced Sagnac sensitivity, *Nature (London)* **576**, 70 (2019).

[33] B. Peng, Ş. K. Özdemir, S. Rotter, H. Yilmaz, M. Liertzer, F. Monifi, C. M. Bender, F. Nori, & L. Yang, Loss-induced suppression and revival of lasing, *Science* **346**, 328 (2014).

[34] W. Liu, Y. Wu, C.-K. Duan, X. Rong, & J. Du, Dynamically Encircling an Exceptional Point in a Real Quantum System, *Phys. Rev. Lett.* **126** 170506 (2021).

[35] H. Xu, D. Mason, L. Jiang, & J. G. E. Harris, Topological energy transfer in an optomechanical system with exceptional points, *Nature (London)* **537**, 80 (2016).

[36] J. Doppler, A. A. Mailybaev, P. Rabl, N. Moiseyev, & S. Rotter, Dynamically encircling an exceptional point for asymmetric mode switching, *Nature (London)* **537**, 76 (2016).

[37] X.-L. Zhang, S. Wang, B. Hou, & C. T. Chan, Dynamically Encircling Exceptional Points: In situ Control of Encircling Loops and the Role of the Starting Point, *Phys. Rev. X* **8**, 021066 (2018).

[38] Q. Liu, S. Li, B. Wang, S. Ke, C. Qin, K. Wang, W. Liu, D. Gao, P. Berini, & P. Lu, Efficient Mode Transfer on a Compact Silicon Chip by Encircling Moving Exceptional Points, *Phys. Rev. Lett.* **124**, 153903 (2020).

[39] A. Li, J. Dong, J. Wang, Z. Cheng, J. S. Ho, D. Zhang, J. Wen, X.-L. Zhang, C. T. Chan, A. Alú, C.-W. Qiu, & L. Chen, Hamiltonian Hopping for Efficient Chiral Mode Switching in Encircling Exceptional Points, *Phys. Rev. Lett.* **125**, 187403 (2020).

[40] J. W. Yoon, Y. Choi, C. Hahn, G. Kim, S. Ho Song, K.-Y. Yang, J. Yub Lee, Y. Kim, C. S. Lee, J. K. Shin, H.-S. Lee, & P. Berini, Time-asymmetric loop around an exceptional point over the full optical communications band, *Nature (London)* **562**, 86 (2018).

[41] T. Gao, E. Estrecho, K. Y. Bliokh, T. C. H. Liew, M. D. Fraser, S. Brodbeck, M. Kamp, C. Schneider, S. Höfling, Y. Yamamoto, F. Nori, Y. S. Kivshar, A. G. Truscott, R. G. Dall & E. A. Ostrovskaya, Observation of non-Hermitian degeneracies in a chaotic exciton-polariton billiard, *Nature (London)*, **526**, 554 (2015).

[42] M. S. Ergoktas, S. Soleymani, N. Kakenov, K. Wang, T. B. Smith, G. Bakan, S. Balci, A. Principi, K. S. Novoselov, Ş. K. Özdemir and C. Kocabas, Topological engineering of terahertz light using electrically tunable exceptional point singularities, *Science* **376**, 184 (2022).

[43] F. Minganti, A. Miranowicz, R. W. Chhajlany, & F. Nori, Quantum exceptional points of non-Hermitian Hamiltonians and Liouvillians: The effects of quantum jumps, *Phys. Rev. A* **100**, 062131 (2019).

[44] W. J. Chen, M. Abbasi, B. Ha, S. Erdamar, Y. N. Joglekar, K. W. Murch, Decoherence Induced Exceptional Points in a Dissipative Superconducting Qubit, *Phys. Rev. Lett.* **128**, 110402 (2022).

[45] M. Naghiloo, M. Abbasi, Y. N. Joglekar, & K. W. Murch, Quantum state tomography across the exceptional point in a single dissipative qubit. *Nat. Phys.* **15**, 1232 (2019).

[46] L. Xiao, K. Wang, X.Zhan, Z. Bian, K. Kawabata, M. Ueda, W. Yi, and P. Xue, Observation of Critical Phenomena in Parity-Time-Symmetric Quantum Dynamics, *Phys. Rev. Lett.* **123**, 230401 (2019).

[47] S. Khandelwal, N. Brunner, & G. Haack, Signatures of Liouvillian Exceptional Points in a Quantum Thermal

Machine, *Phys. Rev. X. Quantum.* **2**, 040346 (2021).
[48] W. J. Chen, M. Abbasi, Y. N. Joglekar, & K. W. Murch, Quantum Jumps in the Non-Hermitian Dynamics of a Superconducting Qubit, *Phys. Rev. Lett.* **127**, 140504 (2021).
[49] S. N. Shevchenko, S. Ashhab & F. Nori, Landau-Zener-Stückelberg interferometry, *Phys. Rep.* **492**, 1 (2010).
[50] L. Landau,, *Phys. Z. Sowjetunion* **2**, 46 (1932); C. Zener, Proc. R. Soc. Lond. A **137**, 696 (1932).
[51] E. C. G. Stückelberg, *Helv. Phys. Acta* **5**, 369 (1932).
[52] F. Zhou, L. L. Yan, S. J. Gong, Z. H. Ma, J. Z. He, T. P. Xiong, L. Chen, W. L. Yang, M. Feng & V. Vedral, Verifying Heisenberg's error-disturbance relation using a single trapped ion, *Sci. Adv.* **2**, e1600578 (2016).
[53] T. P. Xiong, L. L. Yan, F. Zhou, K. Rehan, D. F. Liang, L. Chen, W. L. Yang, Z. H. Ma, M. Feng & V. Vedral, Experimental verification of a Jarzynski-related information-theoretic equality using a single trapped ion, *Phys. Rev. Lett.* **120**, 010601 (2018).
[54] L. L. Yan, T. P. Xiong, K. Rehan, F. Zhou, D. F. Liang, L. Chen, J. Q. Zhang, W. L. Yang, Z. H. Ma, and M. Feng, Single-atom demonstration of quantum Landauer principle, *Phys. Rev. Lett.* **120**, 210601 (2018).
[55] J. W. Zhang, K. Rehan, M. Li, J. C. Li, L. Chen, S. L. Su, L. L. Yan, F. Zhou, & M. Feng, Single-atom verification of the information-theoretical bound of irreversibility at the quantum level, *Phys. Rev. Research* **2**, 033082 (2020).
[56] See Supplementary Material for more detailed results of experimental implementation and theoretical analysis, which includes Refs. [43, 55, 57–59].
[57] Florentin Reiter and Anders S. Sϕrensen, Effective operator formalism for open quantum systems, *Phys. Rev. A* **85**, 032111 (2019).
[58] H. T. Quan, Yu-xi Liu, C. P. Sun, and Franco Nori, Quantum thermodynamic cycles and quantum heat engines, *Phys. Rev. E* **76**, 031105 (2007).
[59] T. Baumgratz, M. Cramer, and M. B. Plenio, Quantifying Coherence, *Phys. Rev. Lett.* **113**, 140401 (2014).
[60] J. Huber, P. Kirton, S. Rotter, & P. Rabl, Emergence of $\mathcal{PT}$-symmetry breaking in open quantum systems, *SciPost Phys.* **9**, 52 (2020).
[61] Y. Nakanishi, & T. Sasamoto, PT phase transition in open quantum systems with Lindblad dynamics, *Phys. Rev. A* **105**, 022219 (2022).
[62] H. Shen, B. Zhen, and L. Fu, Topological Band Theory for Non-Hermitian Hamiltonians, *Phys. Rev. Lett.* **120**, 146402 (2018).
[63] K. Kawabata, T. Bessho, and M. Sato, Classification of Exceptional Points and Non-Hermitian Topological Semimetals, *Phys. Rev. Lett.* **123**, 066405 (2019).
[64] M. Abbasi, W. Chen, M. Naghiloo, Y. N. Joglekar, and K. W. Murch, Topological Quantum State Control through Exceptional-Point Proximity, *Phys. Rev. Lett.* **128**, 160401 (2022).
[65] For example, one may employ the vibrational modes of the ion (used as the working substance) or additional ions confined in the same trap as quantum loads. The positive (or negative) work as illustrated in the text for the ion used as the working substance can be transferred to these quantum loads forming heat current in a microscopic system (or cooling qubits for quantum computing). We note that correlations may be generated between the quantum engine and the quantum load when they are coupled during the iso-decay strokes. Therefore, one should consider pros and cons of such correlations when studying energy transfer and storage, evaluating the thermodynamical processes, and preparing quantum information processing systems.